Perceptual performance and V1 neural activity are exquisitely sensitive to small changes in thalamocortical gain

Veronica C. Galvin[1], Anita A. Disney[1]

[1]Department of Neurobiology, Duke University, Durham, NC, 27710

Corresponding author email address: anita.disney@duke.edu

Acknowledgements: This work was supported by NIH grants R01EY029663 to AAD and F32EY034772 to VCG. The authors gratefully acknowledge the assistance of L. Beaver, J. Amodeo, T. Nguyen, K. Coates and A. Brigande and the veterinary and husbandry staff of the Duke Primate Vivarium for assistance with care and training of the animals used in this study.

Author Contributions: AAD designed the experiments, developed the adaptation of the normalization model, and assisted with analysis. VCG executed the experiments and analyzed the data. AAD and VCG co-wrote the manuscript.

Abstract

Neuromodulators powerfully shape circuit function via mechanisms that largely remain to be determined. As arguably the best-described cortical model system in neuroscience, the primary visual cortex (V1) of the rhesus monkey is an ideal model system to ask and answer these questions. There has been particular focus on acetylcholine actions in V1, where there is strong innervation from the basal forebrain and well-described local cholinergic anatomy in which β2 subunit-containing (high affinity) nicotinic receptors are strongly expressed on thalamocortical axons arriving in layer 4C. Activating these receptors strongly enhances local gain, but it is not known to what extent these effects propagate to other V1 layers. To determine the magnitude and direction (enhancement vs suppression) of gain effects outside layer 4C following gain injection via the nicotinic receptors on thalamic axons, we recorded across the cortical depth in V1 while selectively delivering nicotine locally to layer 4C. We observed widespread and heterogeneous gain effects across layers that could not be explained by visual stimulus conditions, but were well predicted by an adaptation of a normalization model. These gain changes were not compensated by the circuit, and thus were evident during performance of a perceptual task.

Introduction

Neuromodulators play a key role in many, if not all, cortical and subcortical circuits, and disruptions of these systems at various levels (neuromodulator release, receptor expression, reuptake, etc.) can cause profound disruptions to circuit function[1–9]. Understanding the role neuromodulators play is thus essential to understanding virtually all aspects of brain function. The neuromodulator acetylcholine (ACh) has been an area of early and continued focus in this space, as ACh is implicated in sleep/wake cycles, arousal, attention, learning and memory, and in a number of neurological diseases[10–15].

A particular focus of research has been the possibility that ACh supports attentive processing of sensory stimuli [16–22]. In the primate visual system, attention has been shown to increase the sensitivity and selectivity of neuronal responses. While often modeled as glutamatergic feedback from higher-order areas like the frontal eye fields (FEF), the effects of attention on single-unit activity in the primary visual cortex, V1[23–25], are remarkably similar to those induced by cholinergic modulation[16,17]. Overall, ACh is proposed to facilitate "effortful" processing during vigilance states [18,22,26], with extracellular concentrations in the cortex increasing in response to heightened task demands. In V1 specifically, this modulatory signal is positioned to act at the first stage of cortical processing, the thalamocortical synapse [17].

ACh acts via both ionotropic (nicotinic) receptors (nAChRs) and metabotropic (muscarinic) receptors, and innervation from cholinergic nuclei in the basal forebrain and brainstem is widespread throughout cortex[27]. There already exists a strong basis for understanding cholinergic modulation of attentive visual processing in the visual cortex in macaque monkeys, where studies of the precise anatomical localization of both nicotinic and muscarinic receptors indicate that nicotinic receptors are poised to impact incoming sensory signals from thalamus[17] while muscarinic receptors are more widespread throughout the circuit and predominantly expressed on inhibitory neurons[28,29]. In particular, activating nAChRs expressed on thalamic terminals in the primary input layer of V1, layer 4C, enhances gain; likely due to increased glutamate release per action potential [17]. Manipulating nicotinic or muscarinic receptors outside of layer 4C while recording nearby neurons has mixed effects [17,30]. These previous anatomical and physiological findings reveal a mechanism for enhancing feedforward activity at the "gate" to the visual cortex (i.e. layer 4C), but it remains unclear how these local gain changes in the input layer propagate through the V1 circuit and interact with the broader normalization pools that govern activity in the supragranular and infragranular layers. And it is unclear whether and how these effects are related to attention, which ACh is hypothesized to support.

The diverse effects of attention on neuronal gain—variably reported as changes in contrast gain, response gain, or both—have been unified under the framework of divisive normalization. Divisive normalization is widely considered a "canonical neural computation" [31], originally proposed to explain nonlinearities in responses of V1 neurons such as contrast saturation and non-specific suppression [32]. This computational principle, where a neuron's excitatory drive is divided by the pooled activity of its neighbors, is now understood to operate across sensory modalities and species. Two prominent models—from Reynolds and Heeger [33] and Lee and Maunsell [34]—simultaneously proposed that attention works by modulating this normalization machinery. These models demonstrate that the specific form attentional modulation takes (e.g., response vs. contrast gain) emerges from the relative spatial and featural scales of the "attention field" and the stimulus. Overall, these normalization models reconcile a range of reported effects of attention on neuronal activity and yield key predictions for how individual neurons within a population will respond to changes in an attentional "field" but have yet been deployed in service of circuit-level biological insight.

The current study sought to characterize how the effects of a gain injection to layer 4C propagate through the V1 circuit, and further serves as a "causal test" of normalization models of attention. By injecting a spatially and featurally precise gain field into the input layer (by selectively activating the nAChRs on thalamic terminals), we observe how the V1 circuit responds—not just to the visual stimulus, but to the inherited modulatory "attention field". To do this, we conducted two sets of experiments. In the first, we recorded from the full cortical depth while selectively delivering nicotine within layer 4C, simulating a very small attention "field" with tuning determined by the neurons at the site of nicotine delivery. We observed substantial and

highly heterogeneous changes in contrast responses across the cortical column in response to this manipulation. And so, in a second set of experiments, we tested whether the circuit compensates for these exogenously applied gain changes, or whether they 'leak' into behavior during a task designed to test the perceived contrast equivalence of two Gabor stimuli.

Results

While it has been shown across multiple species and brain areas that nAChRs are expressed at thalamocortical synapses onto excitatory (but not inhibitory) neurons, and that direct activation of these receptors using nicotine strongly enhances thalamocortical gain [17,35–39], this effect has not yet been demonstrated in a behaving animal. We thus first sought to assay the local (i.e. within-layer) effect on neural contrast response functions (CRFs) of activating nAChRs in the primary thalamic recipient layer, 4C, of V1 in awake and fixating animals (Fig. 1). Once this local effect was determined, we looked at how these gain changes propagate to alter CRFs recorded in other V1 layers. We used 32-channel linear electrodes equipped with a fluid capillary exiting between electrodes 16 and 17 (Fig. 1C) to deliver nicotine to and simultaneously record from the entire cortical depth of V1. While β subunit-containing nAChRs (i.e. those with a high affinity for nicotine) are expressed almost exclusively at thalamocortical synapses in macaque V1[17], we nonetheless took care to place the fluid port within the borders of layer 4C, based on a current source density analysis of visually-evoked local field potentials.

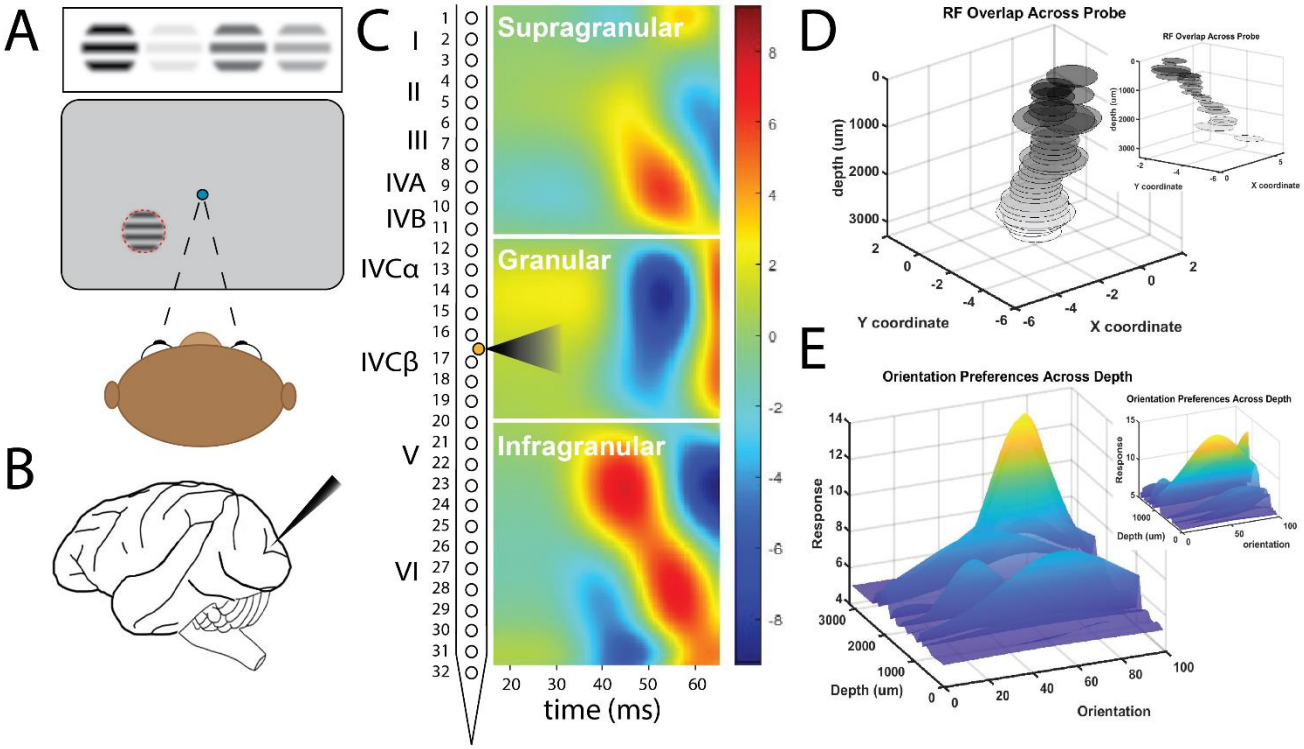

Figure 1. Experimental Design. (A) Schematic of task. Animal fixates within 1.0 degree of visual angle of a central fixation point while Gabor stimuli are presented for mapping of receptive field position, orientation tuning, and contrast responses. (B) Recording units were all within the parafoveal (<8 degrees eccentricity) representation on the opercular surface of the primary visual cortex, V1. (C) S-Probe (Plexon) arrays were inserted perpendicular to the pial surface and positioned to span cortical depth. Based on a current source density analysis of visually-evoked field potentials, a fluid capillary with exit port (yellow dot) between electrodes 16 and 17 (left) was positioned in the granular layer, 4C, for local drug delivery by pressure ejection (black triangle). (D) Receptive field positions were usually well aligned, consistent with a columnar recording. Here shown are our best (main) and worst (inset) aligned recording days. Depth axis: 0 = pial surface/channel 1; 3200um = channel 32. (E) Orientation tuning for the same recording days in D - i.e. most (main) and least (inset) perpendicular.

We recorded 28 single- (SU) and 304 multi-units (MU) across 8 recording sessions; 4 each from one male (164 SU/MU) and one female (64 SU/MU) rhesus monkey. Of these, 143 'units' (i.e. SU and MU activity) were in the supragranular layers (2-4B), 86 were in the granular layer (4C), and 105 were in the infragranular layers (5, 6). A necessary condition for assaying changes in contrast response during drug delivery is demonstrating recording stability during ejection of the drug diluent (in this case saline).

Stationarity of recording during fluid delivery

Delivering saline by pressure ejection can, on its own, cause a loss of unit isolation and a significant decrease in detected spikes up to 6 electrodes away from the fluid capillary (usually 2 or 3). However, after the first few saline 'pulses' in the train (see Methods), the recording generally stabilized and showed excellent stationarity over repeated saline delivery from there forward (Fig. 2A). Forty units (12%) units continued to be non-stationary across the sequence of saline controls, and were discarded, as were units with loss of stimulus driven activity during saline delivery. For the remaining units, we set spike sorting parameters for the whole experiment from an initial saline condition, using this as the baseline from which we then measured changes arising from delivery of nicotine (Fig. 2A,B).

The local effect of nicotine in layer 4C

After discarding non-stationary recordings, 33 units remained for the analysis of gain changes local to 4C, which is the layer in which thalamic axons expressing nAChRs are found in macaque V1[17]. A contrast response function (CRF), which shows the relationship between stimulus intensity and spiking response, is a powerful tool for measuring the gain of visual responses. To first make a non-parametric determination of the overall effect of nicotine delivery we calculated a 'normalized response area' (RA) under the CRF, defined as the ratio for volume-matched nicotine and saline conditions of the sum of the blank-subtracted spike rate across all measured contrasts [17]. After exclusion of non-stationary units, the RA in layer 4C was slightly lower for the saline control trials than for a series of (no fluid delivery) baseline trials (Fig. 2D, light purple, S:B), reflecting a small and stable loss of spikes after the first delivery pulses. The mean RA between the saline control and no-fluid baseline showed a slight reduction for the 81 supragranular (0.9, CI [0.8517 0.9577] one sample t-test) and 50 infragranular (0.9, [CI 0.8352-0.9656], one sample t-test) units that remained after exclusion of non-stationary recordings. Most importantly, the RA was unchanged for all three laminar compartments during repeated delivery of saline, including in an extended control study involving over 1-2 hours of pulsed delivery of saline during recording (supragranular, granular/4C, infragranular; Fig. 2D, dark purple, S:S).

On this background of weak apparent suppression in layer 4C (Fig. 2C), the RA was significantly increased with delivery of nicotine (Fig. 2B,D). Response area variance during nicotine delivery differed significantly from both the baseline (no fluid) and saline controls (Bartlett's test, Fig. 2D, center). The average RA of 1.2 (SEM+/-0.05; yellow asterisks and SEM bars, Fig. 2C) is similar to that observed for ejection currents of 20-80nA in a previous study using iontophoretic delivery of nicotine in layer 4C of macaque V1 under anesthesia[17].

The effect of delivering nicotine to layer 4C on responses in other layers

Given that both the magnitude and direction of the local gain change in layer 4C with delivery of nicotine are similar to those observed in numerous prior studies, we went on to ask what happens to responses in supragranular and infragranular layers that receive this modified layer 4C activity as feedforward drive. We restricted our analyses to units with well-defined, orientation-tuned receptive fields (RF, see Methods) for which the firing rate in response to a 96% contrast best-match stimulus was at least 1 standard deviation above the mean firing rate in response to a blank screen. After applying these criteria, and the stationarity criteria above, 81 supragranular and 50 infragranular units remained for analysis.

Starting with the same non-parametric approach as above, the RA during delivery of nicotine into layer 4C varied enormously across extra-granular units (response area range: 0.13 to 3.98), including a number of

units with no net change (Fig. 2D). We defined an effect range indistinguishable from no net effect based on the range of response areas observed for the above-mentioned 1-2 hour saline stationarity study. This resulted in a 'no net effect' response area range of 0.62 to 1.1 (n = 20 saline control sites; Fig. 2C). 35 supragranular units with response areas >1.1 were classified 'enhanced' and 15 units with response areas <0.62 were classified 'suppressed'. The remaining 29 were classified 'no net effect'. In the infragranular layers, applying the same criteria yielded 25 enhanced, 5 suppressed, and 13 no net effect units (Fig. 2B,D).

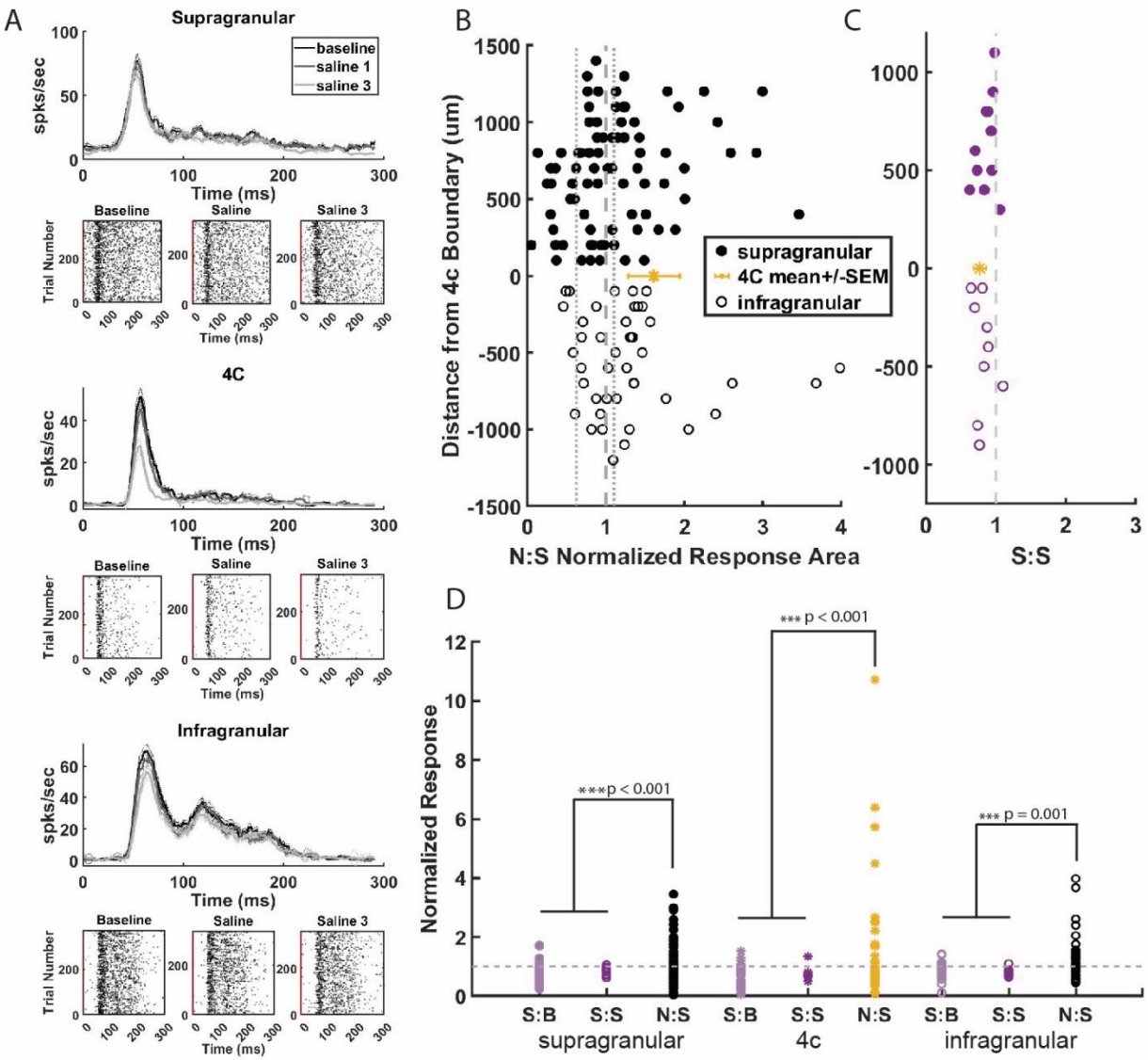

Figure 2. Recording stationarity and population drug effects. (A) Examples of supragranular (top), granular/4C (middle) and infragranular (bottom) responses to repeated saline delivery. The upper panel in each is a sliding window average (10ms) +/- SEM with 0ms indicating stimulus onset. Lower panels are raster plots of every trial across each condition. Baseline: no fluid delivered. Saline: saline delivered via pressure ejection using low (saline 1) and high (saline 3) backing pressure. Saline delivery results in lower spike detection in 4C, but not in other layers. (B) Nicotine causes a net gain enhancement in layer 4C (yellow asterisk) and bi-directional changes to normalized response area in the supragranular (filled circles) and infragranular (open circles) layers. Gray dotted lines indicate the range of values observed in the saline stationarity control shown in panel C. A normalized response of 1 (gray dashed line) indicates no overall difference in spike rate between nicotine and saline conditions. (C) Normalized response area across repeated deliveries of saline (yellow asterisk: mean and SEM for 4C; closed circles: supragranular; open circles: infragranular). (D) Comparison of normalized response area across laminar categories and conditions. Light purple: ratio of Saline to Baseline (S:B). Dark purple: ratio of final Saline repeat to first Saline repeat (S:S). Black (yellow for 4C): ratio of matched pressure and volume Nicotine to Saline (N:S) conditions. p-values: Bartlett's test for homoscedasticity.

Even though high-affinity nAChRs are rarely found outside layer 4C in macaque V1[17], we wondered the extent to which these effects might be explained by nicotine 'wicking' up and/or down the electrode shaft (which is known to occur with these recording devices; our own and others' unpublished observations). Unsurprisingly given the known expression of nAChRs in V1, the magnitude and direction of the change in RA were unrelated to the distance from the 4C boundary (Fig. 2B).

The origin of the heterogeneity in extra-granular response to increased 4C gain

We wondered whether the pattern of response enhancement versus suppression across the population might be explained by the extent to which each site was strongly or poorly driven by the 'best-match' stimulus we chose (see Methods). However, neither gain change magnitude nor direction was correlated with difference between a recording site's preferred orientation and presented stimulus orientation (Fig. 3A) or with the proportion of the receptive field (RF) that overlapped with the visual field location of the stimulus (Fig. 3B). Note that even for the subset of units with 100% RF overlap, a wide range of response magnitudes was observed, encompassing both suppression and enhancement (Fig. 3B, inset). This result is not changed if we restrict analysis to units for which the orientation preference was within 20° of the presented stimulus (considering all RF positions) or to units for which the RF overlap with the stimulus location was at least 90% (considering all orientations; see Supplementary Figure 1).

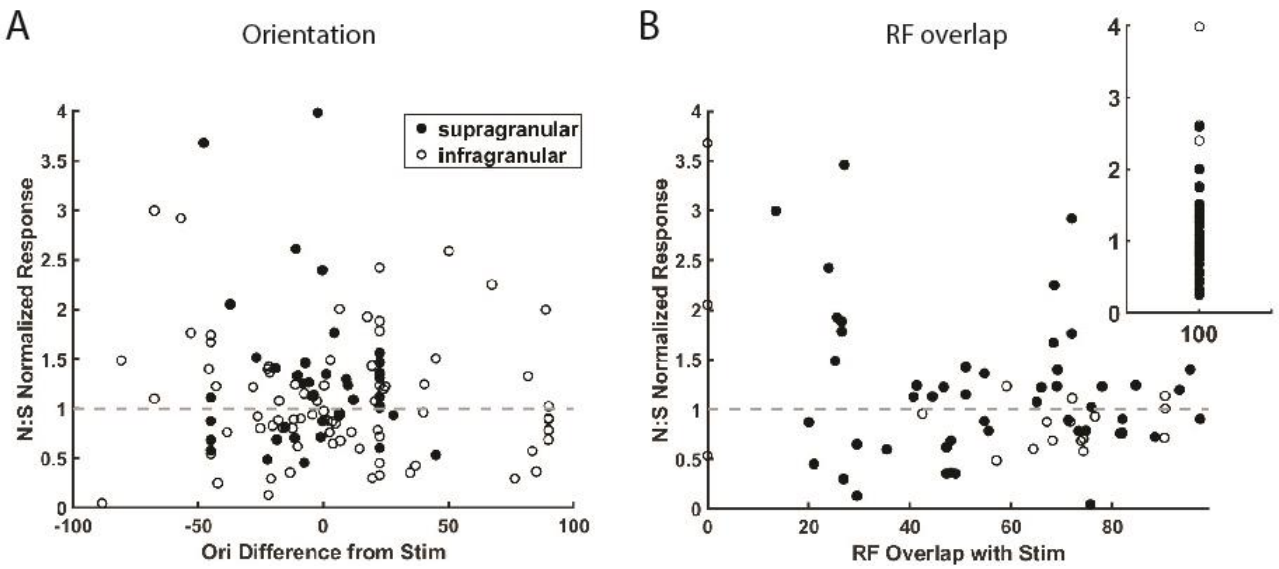

Figure 3. Gain change direction and magnitude are not explained by differences in tuning. (A) Normalized (N:S) response area as a function of the difference between a recording site's preferred orientation and the orientation of the presented stimulus. Horizontal dashed line indicates a normalized response area of 1, or no net nicotine effect. (B) Normalized response area as a function of receptive field overlap. Inset shows the subset of units with 100% overlap.

A parametric analysis of the relationship between stimulus contrast and firing rate is often achieved by fitting a model function to the data in a manner that can yield insight into not only whether gain has changed (as the non-parametric analysis above can do), but in what way[17,40,41]. We wondered whether there might be systematic differences in the form, rather than the magnitude or class, of gain changes across the population and so we fit our data with a hyperbolic ratio function that yields four parameters: slope (n), asymptotic firing rate (Rmax), the contrast at half maximum firing rate (c50), and offset (sFR; see Methods). To quantify changes, for each site we drew a random blank-subtracted spike rate from available trials at each contrast, and fit these data. Repeating this sampling 1000 times, we compared the distribution of values for Rmax (response gain) and c50 (contrast gain) across units and conditions (baseline/saline/nicotine). Similar to our

nonparametric analyses, we saw both enhancement and suppression for response (Rmax change), contrast (c50), and mixed gain effects (in which both Rmax and c50 change), with no clear relationship to visual stimulus or circuit parameters (such as laminar position, distance from the drug delivery site, orientation tuning peak or bandwidth, receptive field size, overlap or position; data not shown).

Applying a Normalization Model of Attention

To this point, we have been approaching the heterogeneity in gain effects across our population like vision scientists; attempting to explain differences in visual responses between our nicotine and saline conditions based on the V1 circuit (e.g. laminar position) and/or the properties of the stimulus. But these are not what differs between our conditions; what changes is that in the nicotine condition, we are injecting a fairly intense, spatially precise (i.e. in a very small region of cortex, <<1 cubic mm) gain pulse to a subset of the neurons responding to the on-screen stimulus. That is, in our experiment, the number of neurons directly affected by the drug is much smaller than the number of neurons driven by the stimulus. Normalization models of attention specifically address such a case[33,34]. Seeking explanation for the observation that sometimes visual attention yields a contrast gain change, and at other times a response gain change, these models formulate the problem in terms of the relative sizes of a gain field (altering responses specific to an attended location) and a stimulus field (the responsive population of neurons as a function of receptive field position and tuning relative to the on-screen stimulus). In their analyses, they find that a multiplicative response gain change arises in the regime in which the relative sizes of these fields are such that stimulus>>attention, predicting changes strikingly similar to those reported previously for nicotine effects in layer 4C [17].

These models modify standard normalization models that have been very successful in describing and predicting visual responses to a range of stimulus conditions[31,32,42]. The standard model proposes that a neuron's response to a stimulus array is normalized by some population of its neighbors. The numerator in that normalization depends on receptive field tuning, so on things like the position and orientation of the stimulus, and the denominator depends on contrast, or activity level. In the attention model, an additional attention field is added as a drive in a manner that modifies both the stimulus and normalization pool responses (Fig. 4A and[33]).

We wondered the extent to which such a model could account for our data and in considering this realized that our data actually represent a model test that would, under most circumstances, be difficult to achieve. Equation 1 gives the model as presented by Reynolds and Heeger[33]:

$$R(x\theta) = |[A(x,\theta)E(x,\theta)]/[S(x,\theta)+\sigma]|_{\mathrm{T}} \qquad \text{Eq. 1}$$

It roughly states that the response, R, of a neuron at spatial position, x, and with preferred orientation, θ, is determined by the ratio of its excitatory drive E(x,θ) to a broadly pooled suppressive signal S(x,θ) and a semisaturation constant, σ, that governs contrast sensitivity. Attention is implemented as a multiplicative gain field A(x,θ), then divided by the suppressive signal. The result is thresholded (T) at zero (for further details see[33]). This model asserts that the attention field is a multiplicative gain term applied to the population of neurons responsive to the stimulus (E(x,θ)) which is inherited by (not directly applied to) the normalization pool (S(x,θ)). A causal test of this claim is extraordinarily difficult to achieve in a behaving primate (human or non-human), but in activating ligand-gated cation channels *selectively expressed on the thalamic terminals* providing input to *excitatory but not inhibitory* thalamic-recipient neurons, in a manner shown to yield a multiplicative gain increase [17], this is in fact the experiment we did. And of course the neurons in the supragranular and infragranular layers don't 'know' that we used nicotine to achieve this; they just see the extra spikes coming through from layer 4C.

So, we decided to apply this model to our data using their publicly-accessible code (see Methods). Critical in a proper model adaptation is considering the ways in which our experiment differs from those the model seeks to explain (see Methods and Supplementary Fig. 2 and Supplementary Table 1 for implementation detials). Briefly, Reynolds and Heeger[33] consider the case in which the stimulus field and attention field are co-located (as a result of 'attending to' the stimulus) and they read out the response (behavioral performance) for that

location. In our experiment, the nicotine field location is determined by the tuning of neurons near the fluid port and does not align perfectly with the stimulus field (chosen as a consensus stimulus to drive neurons across the array, see Methods). Furthermore, the readout is from recording sites that vary in their relative position and tuning with respect to both the stimulus and nicotine fields. And the form of these mis-alignments differs across days (Fig. 1D,E; Fig. 4B).

We moved our data into the model's unidimensional spatial coordinates by projecting each site's RF location onto a vector running from the fixation point through the center of the stimulus position to yield x, and expressed all orientation preferences (θ) as deviations from the presented stimulus (i.e. stimulus orientation = 0°). The projection of RF location (see Methods) yields positions in units that are roughly 2x the eccentricity in degrees of visual angle. We first estimated the RF position and orientation tuning around the fluid port, as priors on the position (Ax) and the tuning peak (Aθ) and bandwidth (AθWidth) of the 'attention field'. We fit the model to classified observed response areas (RA <0.99: 'suppressed'; RA >1.10: enhanced; RA 0.99-1.10: 'no net effect') using a hierarchical approach in which circuit-level (e.g. ratio of excitatory versus suppressive regions of modeled V1 receptive fields) and saline condition 'global' parameters (Table 1) were shared across recording sessions while nicotine field parameters (Table 2) were estimated independently for each session using fixed initial estimates for the global parameters. The resulting per-day fit values for peak amplitude (Apeak), baseline gain (Abase), Ax, Aθ, and AθWidth plus the initial global estimates were then passed as priors and the global and per-day parameters alternately optimized, iterating until convergence. Finally, the global parameters were fixed at their converged values (Table 1) and a final per-day refit was performed to yield session-specific values for Apeak, Abase, Aθ, AθWidth, and Ax (Table 2).

Table 1: Global parameters.

Parameter	Value	Fixed or Fit
Saline Ax	0 (fixation)	fixed
Saline Aθ	0 (stimulus orientation)	fixed
Saline Abase*	1	fixed
Saline Apeak*	4	fixed
Saline AθWidth	90	fit
Nicotine AxWidth	2.4	fit
EθWidth**	50	fit
IθWidth**	70	fit

*Five parameters are fit to each day's data: Abase, Apeak, Ax, Aθ, and AθWidth. Gain field contrast (Table 2) is Abase/Apeak. The saline condition is modeled here as corresponding to a "distributed attention", rather than "no attention", condition. Apeak=4 and Abase=1 reflect model convention for this condition (Reynolds and Heeger, 2009). ** Pooling kernels (excitatory, E, and inhibitory, I) for orientation tuning of V1 neurons.

Table 2: Day-by-day parameters. Five parameters are fit to each day's data: Abase, Apeak, Ax, Aθ, and AθWidth. Gain field contrast is Abase/Apeak.

	Nicotine concentration (mM)	Gain field contrast	Gain field position (Ax, Stimx; AU*)	Gain field tuning (Aθ; degrees)	Gain field bandwidth (AθWidth; degrees)
April 26	500	0.25	8,8	-5	12
Dec 10	200	0.35	2,4	-16	15
Feb 08	400	0.68	4,4	29	17
Jan13	400	0.25	4,4	19	4
Jan 20	400	0.86	11,10	-3	4
Jun 11	400	0.01	5,6	-137	5
Jun 20	300	0.54	3,4	13	4
May 16	250	0.15	10,10	-55	9

* AU: receptive field positions are in arbitrary units arising from projection onto a vector running from fixation through the center of the stimulus position (Stimx), see Methods. Result is roughly 2 * eccentricity in degrees of visual angle.

The result is a unique model implementation for each recording day (Fig. 4). For a given RF position, the model predicts a mix of enhancement, suppression, and net-zero gain effects, largely determined by the recorded neuron's orientation tuning preference (Fig. 4B). Across RF positions, this produces a family of predicted gain curves for the nicotine and saline conditions (shown for the stimulus RF position in Figure 4B), to which we can apply ratio measures to yield per-site model prediction for enhancement, suppression, or no net effect resulting in a predicted gain change surface (Fig. 4C). Note that our columnar recordings mean we sample a small subregion of this predicted space (grayed out region in Fig. 4C represents the unsampled space). The predicted gain effects can then be compared to the observed data for that day (Fig. 4E), where predicted and observed ratios were correlated (Rmax: Spearman p=0.0508, n=17; RA: Spearman p=0.039, n=17).

The fitting results speak directly to underlying biology (see Discussion). For example, on one recording day (May 16th), the fluid port was mispositioned in layer 4B. Per our standard methods, we used the orientation tuning for electrodes 16 (peak: 161°) and 17 (peak: 151°) to provide priors for the model's fitting Aθ. Nicotinic receptors are extremely sparsely expressed in layer 4B of V1 in macaque [17]; accordingly, the model converged on an Aθ = -55 (deviation from the presented stimulus of 157.5°). This reflects the tuning at the nearest layer 4C sites where nAChRs might actually be expressed (electrodes 18/19; preferred orientations 103°/106°), not the tuning of the units around the port (Aθ ≈ 0).

Repeating this over all 8 experimental days, the model accurately predicts effect class (enhanced/suppressed/none) for 79% of units when assessing the prediction of the Rmax parameter from the hyperbolic ratio fits (Fig. 5A) and 77% when assessing prediction of RA (Fig. 5B). Predicted and observed ratios were positively correlated (Rmax: Spearman $\rho = 0.59$, $p < 10^{-12}$; RA: $\rho = 0.49$, $p < 10^{-7}$; n = 121).

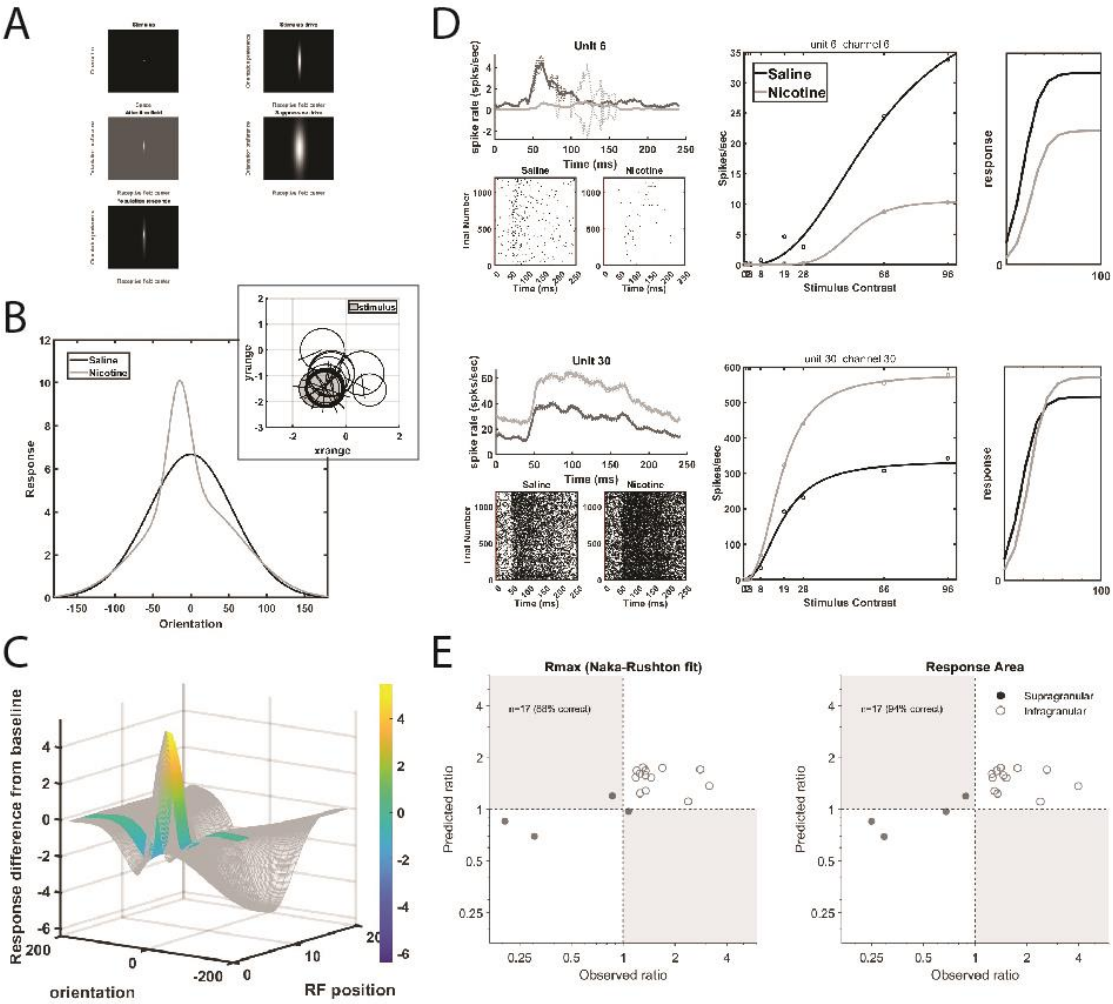

Figure 4. Adapting the Normalization Model of Attention. (A) Adapted from Figure 1 from Reynolds and Heeger[33] using their code modified to reflect our experimental conditions. Note the highly localized 'attention field' representing nicotine delivery at sites in layer 4C with particular RF positions and orientation tuning. (B) Figure made using model code for Figure 5C from Reynolds and Heeger[33], modified to reflect experimental parameters for December 10th (see Table 2). Each curve shows a predicted response magnitude (y-axis) as a function of model neuron tuning, with the 'unattended' (cf saline) condition in black and the 'attended' (cf nicotine) condition in gray. Inset shows the full recording day RF and tuning range overlaid on the presented stimulus (gray). (C) The model-predicted gain change surface for December 10th. The gray surface is the predicted difference over orientation and Ax space (RF position) between the saline and nicotine predictions in B. The section in color indicates the proportion of RF position across our recording probe actually sampled. (D) Example units from December 10th that were suppressed (top) or enhanced (bottom) by nicotine relative to saline. Left panels show a sliding window average+/-SEM for saline (black) and nicotine (gray) for all stimulus presentations (upper) and raster plots for all trials in each condition (lower). Center panels show CRFs fitted with Naka Rushton curves for saline (black) and nicotine (gray). Right panels show model-predicted CRFs. (E) The measured N:S Rmax ratio (x-axis) plotted against the predicted ratio from the model (y-axis) (left). The measured N:S RA (x-axis) plotted against the predicted N:S RA from the model (y-axis) (right). Percentages indicate the number of units from December 10th that are correctly predicted by the model for Rmax (88%) and for RA (94%). n=17. Filled circles: supragranular, open circles: infragranular.

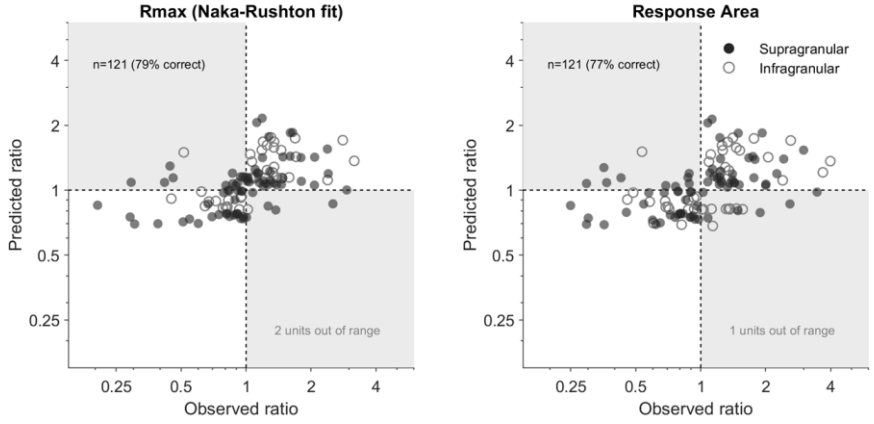

Figure 5. Model prediction versus measured nicotine gain change across the population. (A) Comparison of observed (x-axis) versus predicted (y-axis) ratio of the response to the Rmax of Naka-Rushton fits to contrast response functions for nicotine versus saline. White regions indicate units for which the modeled and measured gain change directions agree; gray regions contain units for which model and measured data diverge. Filled circles: supragranular; open circles: infragranular. (B) Comparison of observed versus predicted RA, conventions as in A.

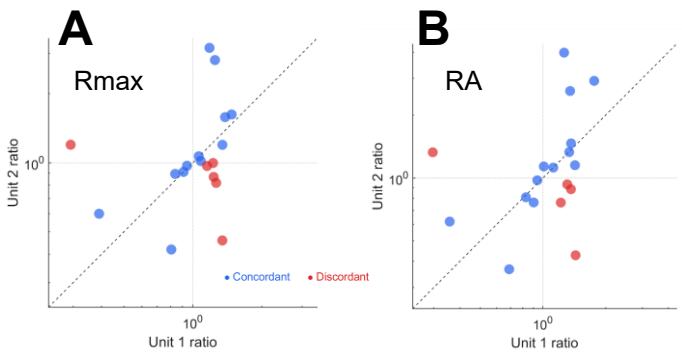

Figure 6. Pair concordance for units recorded on the same electrode. (A) Comparison of the nicotine/saline ratio for the Rmax parameters fit to each unit's contrast response function (CRF), for units recorded on the same electrode (18 units across 6 days, both animals). (B) Same as A for the nicotine/saline ratio of the normalized response area (RA) under the CRF. Blue circles: concordant sites; red circles: discordant sites.

For 18 sites, we had two well-isolated units on the electrode. At 12 of these sites, the Rmax (Fig. 6A) and RA (Fig. 6B) ratios were concordant between the pairs. Concordance within this small sample was unrelated to tuning similarity (not shown).

The gain effects evident in neural activity impact perceptual performance

Our injection of gain within a very small region of layer 4C neurons alters activity across the entire cortical column (Fig. 2). We wondered whether the circuit can compensate for these effects, or whether they will be evident in behavior. We trained one animal (E) on a perceptual equivalence contrast discrimination task requiring comparison of two concurrently presented Gabor stimuli of matched size, orientation, and spatial and temporal frequency. The animal's task was to saccade to the Gabor with higher apparent contrast (Fig. 7A, top). We delivered nicotine to layer 4C during task performance in 6 separate recording sessions (days). On three of these days, the tuning of units in layer 4C was close to the orientation of the presented Gabor stimuli. On these days, behavior during nicotine delivery indicated that a lower contrast stimulus presented in

the contralateral visual hemifield was indistinguishable from the target (evidenced by 50% choice probability) than was the case during saline delivery at the same site (Fig. 7B). On three days when the tuning near the port differed from the stimulus presented, the opposite effect was observed (nicotine yielded equal choice probability for a higher contrast stimulus than under saline; Fig. 7C).

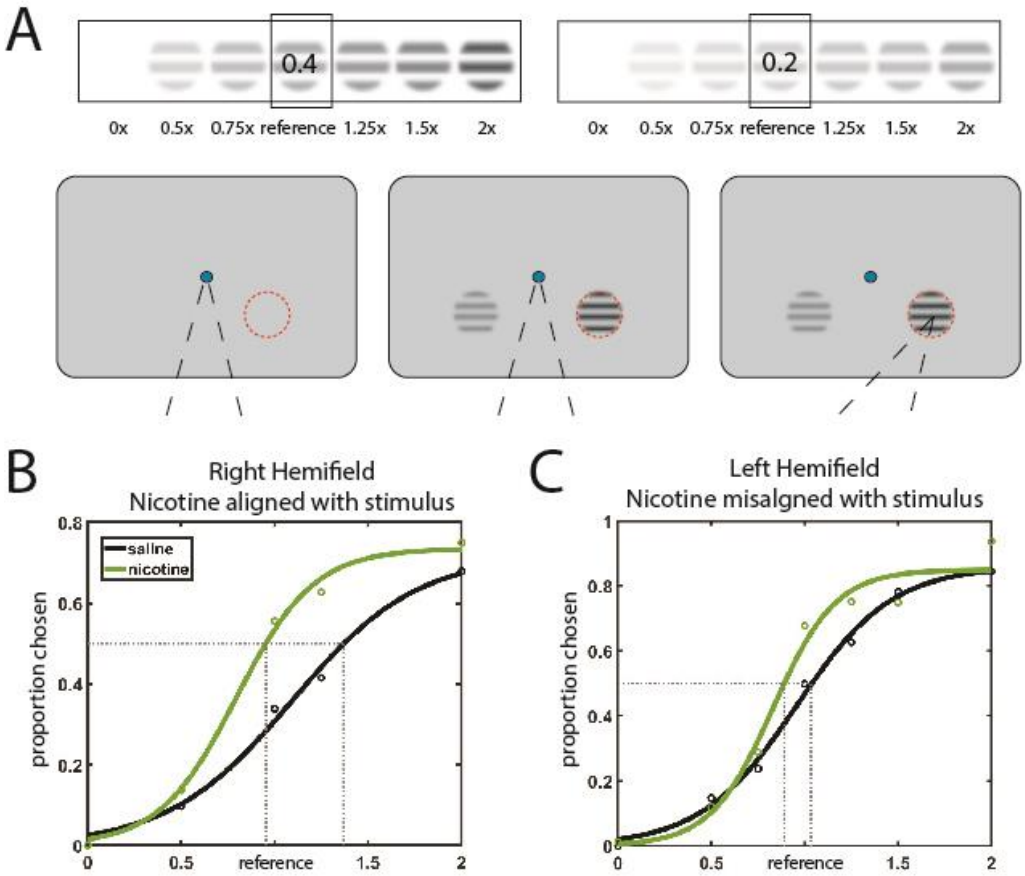

Figure 7. Nicotine delivery in layer 4C alters perceived contrast. (A) Upper panels indicate the two reference contrasts used (20 and 40%) for Gabor stimuli, around which three halfstep comparison target contrasts were generated and presented in randomized order. Lower panels show (from left to right) the task design. Animal fixates on a center point on screen (left), and after a variable time two Gabor stimuli are presented (center), one within the RF position at that day's recording and nicotine delivery site (red dashed circle), and one in the contralateral hemisphere. The animal's task is to report the higher contrast stimulus (right). (B) Choice behavior across three days during which nicotine (green) was delivered to layer 4C sites in left V1 that were co-tuned with the stimulus presented on that day, resulting in biased choice in the (contralateral) right visual hemifield in favor of lower contrast stimuli. Note the animal's overall bias *against* right hemifield choices (curve asymptotes at $p<0.6$ for the saline control, black), which this nicotine effect overcomes. (C) Conventions as in B for three days during which the layer 4C sites in left V1 at which nicotine was delivered were *not* co-tuned with the stimulus. This resulted in biased choice in the (ipsilateral) left visual hemifield in favor of lower contrast stimuli.

Discussion

Here we show that injecting a gain pulse to a small region of cortex yields profound changes in neuronal activity over a much wider swath of tissue, and that these changes are not compensated for, and thus modify perceptual performance. By using laminar arrays to deliver nicotine specifically into the primary thalamic recipient (granular) layer, 4C, while recording from across all layers of primary visual cortex (V1), we first confirmed that activation of nicotinic acetylcholine receptors (nAChRs) in layer 4C locally (i.e. within layer 4C)

increases the responsiveness of neurons (Fig. 2), as been shown previously across species and sensory systems[17,35–37,39]. The anatomical localization of nAChRs in macaque V1, and the direct effect of nicotine release on contrast gain for V1 neurons, revealed in our earlier work [17], provides a basis for interpreting the current study. We found that β2 subunit-containing (high affinity) nAChRs are expressed presynaptically on thalamocortical terminals that synapse onto the spines of excitatory neurons in layer 4C, and are very rarely expressed anywhere else in V1. This expression pattern allows acetylcholine (ACh) to selectively strengthen ascending drive to thalamic-recipient excitatory neurons without increasing the overall excitability of the local circuit. Our interpretation here focuses on the expression of these high affinity nAChRs both because data on the expression of the low affinity (homomeric α7 subunit-containing) nAChRs is not available for V1 (antibodies directed against the α7 subunit have never passed controls in our hands) and because the pattern of functional effects of nicotine delivery in V1 corresponds tightly to the expression pattern of the high affinity receptors[17].

In addition to local gain enhancement near the site of delivery, nicotine induced changes in contrast responses for neurons hundreds of micrometers away, in the supragranular and infragranular layers. It is highly unlikely that distal effects are due to local activation of nAChRs outside layer 4C because local delivery of nicotine in layers 2-4B, 5, and 6 does not alter visual responses [17]. The heterogeneous nature of the effects in other layers highlights a complex interplay between the inherited gain and local cortical circuitry and suggests that the impact of ACh release is not a uniform "volume control" but yields a sophisticated, circuit-dependent computation. We considered the possibility that this computation is a gain field that can be modeled by normalization models of attention [33,34].

Normalization models propose that attention acts by modulating a neuron's excitatory drive relative to a normalization pool of neighboring activity. Our finding that a local gain pulse in layer 4C generates diverse patterns of enhancement and suppression across the column that are well-predicted by a normalization model (Fig. 5) allows us to go on and consider what the specific fit parameters that yield these predictions can tell us about biology.

We *a priori* conceived of the nAChR-mediated gain injection as a tightly tuned field, equivalent to that yielded by focal attention in the normalization models. Accordingly, in initializing our models, the prior on the parameter that captures the size of the attention field (AxWidth) was set to 3, representing a gain field 75% the size of the stimulus (set to a value of 4). Intriguingly, when we went on to fit this as a global parameter, it converged on a value of 2.4—60% the size of the stimulus—which is exactly the ratio of attention:stimulus field that arose in fits to attention data in the original model publication [33], possibly revealing a ‘source-agnostic’ mechanism that determines the spread of gain enhancement within the V1 circuit.

Looking at other global parameters, we find that during the fixation task—which we modeled as a distributed attention, rather than unattended (i.e. attention actively directed elsewhere), condition—endogenous attention spreads across the central ~4 degrees (of visual angle) of the visual field (obtained by converting Saline AxWidth to field coordinates: ~7.5 divided by 2). The gain field in this condition is untuned for orientation (Saline AθWidth = 90), despite the fact that a Gabor of fixed orientation (and size, spatial frequency, etc.) is being presented in the parafoveal field. Per convention [33], we modeled this "distributed attention" regime as having an attention field contrast (Abase/Apeak) of 0.25 with specific values of Apeak = 4 and Abase = 1. Moving to the day-by-day parameters, it is interesting to note that the two days for which the fit gain field ratio was <0.25 (May 16th and June 11th) were days on which the tuning at the port deviated substantially from the presented stimulus (Aθ = -55 and -137, respectively), and the larger the deviation, the smaller the ratio (0.15 and 0.01, respectively). A ratio <0.25 indicates suppression of neurons away from the injection site relative to saline baseline. For days where Aθ was closer to 0, the gain field ratio was not directly predictable from the magnitude of the orientation deviation (Table 2). As noted above, on the one day when we had the fluid port misplaced (in layer 4B), this could be diagnosed from the fit parameters, which converged on gain field tuning corresponding to the tuning for the nearest electrodes that were within layer 4C.

For fit units, we passed the model only the location of the peak of a von Mises fit to spiking responses as a function of orientation. We then allowed the model to fit the excitatory and inhibitory kernels that together define orientation tuning bandwidth as global parameters. The fitted excitatory and suppressive pooling widths (EθWidth = 50° and IθWidth = 70°, expressed as Gaussian σ) are consistent with the normalization model's requirement that suppressive pooling extend more broadly in orientation space than excitatory pooling. The excitatory kernel, which determines the range of orientations contributing to a neuron's feedforward drive, is broader than typical single-neuron orientation bandwidths in macaque V1 (median half-width at half-height of 20–40°[43,44]), as expected for a pooling kernel that integrates across multiple afferents. The suppressive kernel extends approximately 40% further in orientation space, producing the broader-than-excitation normalization pool that underlies orientation-selective responses through divisive normalization[31,32].

The model fits thus appear informative of underlying biology, not simply predictive of gain class for recorded neurons. How seriously should we take this? Our modeling fits 44 parameters for 121 data points, which sounds like a lot. We would note first that the model loss is discrete, not continuous; in fitting to 121 ternary labels (+1, -1, 0), a random model would get ~50% correct. Even though the baseline is high, the 77-79% accuracy we observe represents meaningful structure, and while magnitudes are not fit at all, predicted and observed ratios are correlated (Fig. 5). Further, many of the per-day fit parameters are constrained by independent measurements (Ax RF mapping, Aθ from tuning, near the fluid port), so they aren't fully free in practice, and the global parameters are shared across days, so 4 parameters are explaining structure across all 121 units simultaneously. Finally, the per-day parameters can't trade off against each other—each day's 5 parameters only affect that day's recording sites (typically 10–25 per day).

And so we see rich and complex changes across the neural circuit in response to these tuned gain pulses; our behavioral data (Fig. 7) show that these changes are not compensated for and are passed on to yield biased perceptual performance. To our knowledge, this is the first demonstration of a behavioral effect of such highly localized drug delivery into the cortex of a behaving primate. That these tiny tissue volumes can yield such powerful control of behavior speaks to the power of controlling the ‘gate’ to cortex, a solution biology has found not just for the cholinergic system, but for neuromodulation in general, which is powerfully and specifically directed at this critical point in the circuit[45].

So could this be ‘the’ mechanism of attention? Strictly speaking, almost certainly not: although the capacity of the cholinergic system to specifically address such a precise point (~1mm) in cortex has not been determined (those studies are underway in our lab), it would require some very exotic (although biologically feasible [46]) circuitry to do so. Importantly, however, the neurons outside layer 4C do not ‘know’ that we used nicotine to inject this gain; they just see the additional spikes. And so from that standpoint, our study shows that if you want to achieve tuned contrast enhancement of a visual stimulus (as attention certainly does[24,41,47]), this mechanism would do the job.

Methods

Animals

One adult male (D, age 10) and one adult female (E, age 12) Macaca mulatta were used in this study. Animals were socially-housed in an AAALAC-certified facility at Duke University on a 12-hour light/dark cycle in humidity and temperature controlled environments. All procedures were approved by Duke University's Institutional Animal Care and Use Committee, in accordance with NIH guidelines. Both animals were maintained on ad libitum food and water in their home cages throughout the study.

Behavior

Behavioral control and monitoring: During task performance and recording, animals were seated in a dimly lit (<1 cd/m2) Faraday room and monitored continuously via infra-red camera. Eye position and pupil size were monitored non-invasively using a high-speed infra-red eye tracking system (EyeLink). Visual stimuli were delivered by a ProPixx projector (VPixx) onto the central 73.5 X 40.5 cm of a 122 x 91cm (W x H) polarization-preserving rear projection screen (Stewart Filmscreen) positioned 98.5 cm from the eyes. Animals were head fixed using the Thomas Recording titanium 3-post mini plate + 'Halo' system (Thomas Primate Positioning System).

Passive Fixation Task: Animals were trained to maintain fixation within 1.0 degree of visual angle (dva) of a fixation point at the center of the screen while Gabor stimuli of varying position, orientation, and contrast (fixed diameter=2dva and spatial frequency=1.5 cycles/degree, cpd) were presented for 150ms on/off periods on a 20 cd/m2 mean gray background (Figure 1A). ~0.2mL dilute juice or water reward was delivered for correctly maintaining fixation through the full fixation period.

Perceptual Equivalence Task: Animals were trained to fixate (as described for passive fixation, above). After a period of 750-1750ms, two Gabor stimuli would appear simultaneously, one in each hemifield. Stimuli were identical in size, spatial frequency, temporal frequency, and orientation, but different in contrast (optimized as described for passive fixation, above). Trials were randomly interleaved for two series of contrast comparisons against a) 20% and b) 40% contrast 'target' Gabors. Stimuli for comparison were generated representing three half-steps presented in randomized order using the method of constant stimuli (see Fig. 7). Animals were trained to saccade to the higher contrast stimulus. A juice reward was delivered for correct choices; choices between identical stimuli were randomly rewarded. To prevent reward feedback interfering with possible drug effects on perception, during the nicotine delivery window a probabilistic reward was enacted such that stimuli that differed by 3% contrast or less were rewarded with probability 0.75, regardless of choice.

Behavioral Analysis: Performance was initially split by reference contrast (20% or 40%) and hemisphere and a 'proportion chosen' calculated for each reference-target contrast pair (number of trials target contrast selected/total number of target contrast presentations). The MATLAB Curve Fitting Toolbox was used to fit a Logistic function to behavior, and curves and proportion chosen values were plotted together.

Electrophysiology

The combined electrophysiology and drug delivery experiments were conducted using 32-channel S-Probes (Plexon; PLX-SP-32-15SE(100)-(260-100)(640-30)-640-FC16/17-(1)CON/32m-V). Electrodes were 100um apart and a fluid capillary allowing for drug delivery exited the probe between electrodes 16 and 17 (Figure 1B). Data were recorded using Synapse software from Tucker Davis Technologies (TDT) at a sampling rate of 24414.0625, amplified using TDT PZ5, and TDT RZ2 bioamp processor, band pass filtered (300 Hz to 10 kHz) and stored for offline analysis.

S-Probes were positioned using a motorized drive (Thomas Recording), with a sharpened stainless steel guide tube to assist in passing dura. Dura thickness was measured before the first recordings were made using a single unit electrode, and the approximate thickness estimated based on changes in height from the chamber top. Guide tube tips were positioned just before cortex (i.e. still within dura) and the stainless steel-

tipped S-probe used to exit dura and enter cortex. Electrodes were advanced at a drive speed of 2μm/second until the last channel was estimated to be just above or within layer 1.

Initial depth was determined by current source density (CSD) analysis calculated from a 2-3 minute recording of local field potential responses to 100ms flashes of 100% contrast full-screen gratings (1.5 cpd), presentation of which was initiated any time the eyes were on the screen. Electrode position was adjusted as needed to place the fluid capillary in layer 4C.

Receptive field position was mapped using flashed horizontally- and vertically-oriented Gabor stimuli (2dva, 1.5 cpd, 96% contrast, randomly interleaved). Orientation tuning preference was measured using Gabor stimuli (22.5° steps, randomly interleaved including blanks). Based on the observed receptive field positions and tuning preferences across the recording array, a 'best-fit' stimulus location and orientation were chosen for use in measuring contrast gain. Contrast gain was measured in 9 logarithmic steps from 1% to 96% plus 0% contrast 'blanks' (all randomly interleaved).

Pharmacology:

Nicotine (Glentham Life Sciences; cat#65-31-6) was weighed and mixed in solution with sterile saline, pH adjusted to 4.5-7.0 and filtered at 0.22um prior to loading into electrodes for use. Pre-mixed solution was kept at 4°C for up to 7 days, after which a fresh solution was prepared. Nicotine concentration varied from 200mM-500mM and estimated maximum total volume delivery for a given day was ~1-2μL. Solutions (saline and nicotine) were delivered by pressure ejection (WPI pneumatic PicoPump PV830, or a Medical Systems Corp PLI_100 depending on the rig used for recording). Saline or nicotine delivery occurred between the onset of fixation and presentation of the first stimulus. An electrode-specific pressure range was determined ex vivo based on calibration under a microscope (volume estimation from measured droplet size) and adjusted for each recording using 15 PSI pulses, based on response stationarity (qualitatively assessed) for electrodes flanking the fluid port. Final pressure used for saline and drug delivery ranged from 2.5-20PSI.

Data Processing and Analysis:

Spike recording, sorting, and windowing: Wave forms were sorted offline in MATLAB (MathWorks) using the 'Spike' sorting code developed by Dr. K. Nielsen at Johns Hopkins University. Thresholds were individually set per channel and sorts were based on multiple waveform characteristics (spike amplitude max, spike amplitude min, spike width, etc). Response window start times were calculated for each unit individually by calculating a per-trial baseline (average and standard deviation of spike rate in the first 20ms after stimulus onset) and then finding the first 10ms window during which the average spike rate was more than 2 sd over baseline. The trial response window began 5ms before the start of the initial response bin.

Inclusion criteria for analysis: Permissive inclusion criteria were used. For units (MU or SU) to be used in our analyses they needed to have (1) a clear receptive field position, (2) a spike rate difference >1spk/sec between the peak and trough of the orientation tuning function, (3) an average spiking response to the 96% contrast stimulus at least 1 sd higher than the average response to the 0% contrast blank, (4) an average response to the 96% contrast stimulus under the no-fluid delivery baseline of > 1 spk/sec, and (5) (for supragranular and infragranular only) a response that was not significantly suppressed by saline delivery, determined by an AUC bootstrap analysis (see nonparametric methods). Additional visual inspection of rasters per unit ensured responses to stimuli weren't lost during fluid delivery.

Parametric analysis of contrast responses: A hyperbolic ratio (Naka-Rushton) function (Eq. 2) was fit for each condition (baseline, saline, drug) to the averaged (across 39-247 repeats) responses, R, for each stimulus contrast, C: R=RmaxCnCn+C50n+sFR

This fit yields four parameters: Rmax (maximum response), c50 (contrast at the half-maximum response), n (function slope) and sFR (offset attributable to 'spontaneous' firing). A bootstrap analysis was performed by sampling randomly from responses to each contrast and fitting a Naka-Rushton function. 1000 bootstrap iterations were used to estimate parameter distributions.

Non-parametric analysis of contrast responses: We obtained an approximate 'area under the curve' (AUC) by finding the mean response rate to each contrast and taking the sum of these mean rates across all contrasts. The normalized response area was then calculated as a ratio of AUC values between conditions. An AUC bootstrap analysis was run by randomly sampling responses to each contrast, calculating the sum 1000 times.

Significance testing of bootstrap analyses: Bootstrapped AUC or Naka-Rushton parameter values were randomly sampled from the conditions to be compared and the ratio calculated. If, for example, the saline condition AUC value was less than the baseline AUC value 950 or more times out of these 1000 comparisons, we considered the unit to be significantly suppressed by saline.

Normalization Model of Attention

We used both publicly-available scripts (https://snl.salk.edu/~reynolds/Normalization_Model_of_Attention/) and our own custom MATLAB code for this analysis.

Using port tuning as priors on Ax, Aθ, and AθWidth: The nicotine attention field center was constrained by independent measurements at the fluid port. The spatial center (Ax) was initialized from the receptive field location mapped at the port electrodes (channels 16 and 17, which flanked the capillary port). The orientation center (Aθ) was initialized from orientation tuning measured at the port. To constrain the orientation width (AθWidth) of the attention field, we use the peak location and bandwidth from double von Mises fits to spiking responses as a function of stimulus orientation for four electrodes neighboring the port (channels 15–18). Each von Mises fit measurement was assigned a confidence weight (1.0 for well-isolated units with clear tuning; 0.5 for noisy, weakly tuned, or multiunit estimates; excluded if no responsive units were present) and a distance weight that decayed with electrode distance from the port (channels 16–17 received full weight; more distant channels were downweighted as 1/distance). The circular variance of the weighted orientation preferences provided an empirical estimate of the orientation diversity across the neural population at the nicotine delivery site, which served as a plausibility check on the fitted attention field width (AθWidth). When orientation tuning bandwidth measurements were available (full width at half height of the tuning curve, converted to Gaussian sigma), the mean bandwidth provided an additional constraint on the expected spread (across orientations) of the nicotine gain field.

Fitting the model: We fit the normalization model to the observed nicotine/saline response ratios using a hierarchical optimization procedure. Parameters were divided into two classes: per-session parameters describing the nicotine gain field for each recording day (peak amplitude, Apeak; baseline gain, Abase; orientation center, Aθ; orientation width, AθWidth; and spatial center, Ax), and global parameters shared across all sessions describing the circuit architecture (excitatory and suppressive pooling widths EθWidth and IθWidth, saline field width salθWidth, and nicotine spatial field width nicAxWidth). The model was thus fit with 5 free parameters per session (Apeak, Abase, Aθ, AθWidth, Ax) and 4 shared parameters optimized across sessions (nicAxWidth, salAθWidth, EθWidth, IθWidth), totaling 44 free parameters for 121 observations. Because the loss function operates on sign classifications rather than continuous values, the effective information per observation is less than one bit, making direct comparison of parameter count to observation count conservative — many parameter configurations produce identical sign predictions, and the continuous parameters are further constrained by the port tuning measurements.

For each recording day, each neuron's position in model space was determined by projecting its receptive field location onto the stimulus axis and computing its preferred orientation relative to the stimulus orientation. The model predicted a nicotine/saline response ratio for each neuron by computing the full normalization equation under both nicotine and saline attention field configurations at 96% contrast and across all tested contrasts (for the normalized response area measure). The loss function counted the number of sign mismatches between predicted and observed ratios, classifying each neuron as enhanced (ratio > 1.01), suppressed (ratio < 0.99), or no effect. Optimization proceeded in three stages: first, independent per-session fits were performed with global parameters fixed at initial estimates; second, global and per-session parameters were alternately optimized, iterating until convergence; third, a final per-session refit was performed with the converged global parameters held fixed. To address potential degeneracy between Apeak

and Abase, each independent fit was run along two optimization paths that released these parameters in opposite order, and the lower-loss solution was retained. Abase and Apeak trade-off in determining scaling and are properly considered as a ratio, rather than in absolute terms, so in the text and for model evaluation the attention field contrast (Abase/Apeak) was calculated (reported in Table 2). For model evaluation (below), we fixed the peak amplitude of the nicotine attention field at Apeak = 4, matching the default value in the original Reynolds and Heeger model 33, and calculated Abase from the field contrast (Apeak/Abase ratio). This convention resolves an inherent degeneracy in the normalization model: because both excitatory drive and the suppressive pool are scaled by the attention field, the predicted response ratio depends only on the contrast between peak and baseline gain, not on their absolute values. Fixing Apeak anchors the absolute scale without affecting predictions. This parameterization does not assume a specific correspondence between Apeak and the magnitude of nicotinic receptor activation; rather, it provides a normalized coordinate system in which the spatial and orientation structure of nicotine's modulatory field can be compared across sessions.

Evaluating model performance: Model accuracy was quantified as the percentage of neurons for which the predicted direction of nicotine's effect matched the observed direction. Each neuron was classified as enhanced (nicotine/saline ratio > 1.01), suppressed (ratio < 0.99), or no effect (0.99–1.01) based on both the observed and model-predicted ratios. A prediction was scored as correct if the predicted and observed classes matched. Accuracy was computed separately for the nicotine/saline ratio of the Rmax parameter fit to the hyperbolic ratio (Naka-Rushton) function and of the normalised response area and a Spearman correlation calculated on log-transformed ratios.

References

1. Vijayraghavan, S., Major, A.J., and Everling, S. (2018). Muscarinic M1 receptor overstimulation disrupts working memory activity for rules in primate prefrontal cortex. Neuron *98*, 1256–1268.e4.

2. Chiba, A.A., Bushnell, P.J., Oshiro, W.M., and Gallagher, M. (1999). Selective removal of cholinergic neurons in the basal forebrain alters cued target detection. Neuroreport *10*, 3119–3123.

3. Pinto, L., Goard, M.J., Estandian, D., Xu, M., Kwan, A.C., Lee, S.-H., Harrison, T.C., Feng, G., and Dan, Y. (2013). Fast modulation of visual perception by basal forebrain cholinergic neurons. Nat. Neurosci. *16*, 1857–1863.

4. Azam, L., Chen, Y., and Leslie, F.M. (2007). Developmental regulation of nicotinic acetylcholine receptors within midbrain dopamine neurons. Neuroscience *144*, 1347–1360.

5. Bailey, C.D.C., Alves, N.C., Nashmi, R., De Biasi, M., and Lambe, E.K. (2012). Nicotinic α5 subunits drive developmental changes in the activation and morphology of prefrontal cortex layer VI neurons. Biol. Psychiatry *71*, 120–128.

6. Ballesteros-Yáñez, I., Benavides-Piccione, R., Bourgeois, J.-P., Changeux, J.-P., and DeFelipe, J. (2010). Alterations of cortical pyramidal neurons in mice lacking high-affinity nicotinic receptors. Proc. Natl. Acad. Sci. U. S. A. *107*, 11567–11572.

7. Vitiello, B., Martin, A., Hill, J., Mack, C., Molchan, S., Martinez, R., Murphy, D.L., and Sunderland, T. (1997). Cognitive and behavioral effects of cholinergic, dopaminergic, and serotonergic blockade in humans. Neuropsychopharmacology *16*, 15–24.

8. Croxson, P.L., Kyriazis, D.A., and Baxter, M.G. (2011). Cholinergic modulation of a specific memory function of prefrontal cortex. Nat. Neurosci. *14*, 1510–1512.

9. Bear, M.F., and Singer, W. (1986). Modulation of visual cortical plasticity by acetylcholine and noradrenaline. Nature *320*, 172–176.

10. McCutcheon, R.A., Weber, L.A.E., Nour, M.M., Cragg, S.J., and McGuire, P.M. (2024). Psychosis as a disorder of muscarinic signalling: psychopathology and pharmacology. Lancet Psychiatry *11*, 554–565.

11. Gallagher, M., and Colombo, P.J. (1995). Ageing: the cholinergic hypothesis of cognitive decline. Curr. Opin. Neurobiol. *5*, 161–168.

12. Bakanidze, G., Roinishvili, M., Chkonia, E., Kitzrow, W., Richter, S., Neumann, K., Herzog, M.H., Brand, A., and Puls, I. (2013). Association of the nicotinic receptor α7 subunit gene (CHRNA7) with schizophrenia and visual backward masking. Front. Psychiatry *4*, 133.

13. Sarter, M., Hasselmo, M.E., Bruno, J.P., and Givens, B. (2005). Unraveling the attentional functions of cortical cholinergic inputs: interactions between signal-driven and cognitive modulation of signal detection. Brain Res. Brain Res. Rev. *48*, 98–111.

14. Jiménez-Capdeville, M.E., and Dykes, R.W. (1996). Changes in cortical acetylcholine release in the rat during day and night: differences between motor and sensory areas. Neuroscience *71*, 567–579.

15. Jasper, H.H., and Tessier, J. (1971). Acetylcholine liberation from cerebral cortex during paradoxical (REM) sleep. Science *172*, 601–602.

16. Herrero, J.L., Roberts, M.J., Delicato, L.S., Gieselmann, M.A., Dayan, P., and Thiele, A. (2008). Acetylcholine contributes through muscarinic receptors to attentional modulation in V1. Nature *454*, 1110–1114.

17. Disney, A.A., Aoki, C., and Hawken, M.J. (2007). Gain modulation by nicotine in macaque v1. Neuron *56*, 701–713.

18. Sarter, M., Bruno, J.P., and Givens, B. (2003). Attentional functions of cortical cholinergic inputs: what does it mean for learning and memory? Neurobiol. Learn. Mem. *80*, 245–256.

19. Knudstrup, S.G., Martinez, C., Rauscher, B.C., Doran, P.R., Fomin-Thunemann, N., Kilic, K., Jiang, J., Devor, A., Thunemann, M., and Gavornik, J.P. (2024). Visual stimulation drives retinotopic acetylcholine release in the mouse visual cortex. Neuroscience.

20. Dalley, J.W., McGaughy, J., O'Connell, M.T., Cardinal, R.N., Levita, L., and Robbins, T.W. (2001). Distinct changes in cortical acetylcholine and noradrenaline efflux during contingent and noncontingent performance of a visual attentional task. J. Neurosci. *21*, 4908–4914.

21. McGaughy, J., Dalley, J.W., Morrison, C.H., Everitt, B.J., and Robbins, T.W. (2002). Selective behavioral and neurochemical effects of cholinergic lesions produced by intrabasalis infusions of 192 IgG-saporin on attentional performance in a five-choice serial reaction time task. J. Neurosci. *22*, 1905–1913.

22. Hasselmo, M.E. (1995). Neuromodulation and cortical function: modeling the physiological basis of behavior. Behav. Brain Res. *67*, 1–27.

23. Motter, B.C. (1993). Focal attention produces spatially selective processing in visual cortical areas V1, V2, and V4 in the presence of competing stimuli. J. Neurophysiol. *70*, 909–919.

24. Reynolds, J.H., and Chelazzi, L. (2004). Attentional modulation of visual processing. Annu. Rev. Neurosci. *27*, 611–647.

25. McAdams, C.J., and Reid, R.C. (2005). Attention modulates the responses of simple cells in monkey primary visual cortex. J. Neurosci. *25*, 11023–11033.

26. Hasselmo, M.E., and McGaughy, J. (2004). High acetylcholine levels set circuit dynamics for attention and encoding and low acetylcholine levels set dynamics for consolidation. Prog. Brain Res. *145*, 207–231.

27. Mesulam, M.M., Mufson, E.J., Levey, A.I., and Wainer, B.H. (1983). Cholinergic innervation of cortex by the basal forebrain: cytochemistry and cortical connections of the septal area, diagonal band nuclei, nucleus basalis (substantia innominata), and hypothalamus in the rhesus monkey. J. Comp. Neurol. *214*, 170–197.

28. Disney, A.A., Domakonda, K.V., and Aoki, C. (2006). Differential expression of muscarinic acetylcholine receptors across excitatory and inhibitory cells in visual cortical areas V1 and V2 of the macaque monkey. J. Comp. Neurol. *499*, 49–63.

29. Disney, A.A., and Aoki, C. (2008). Muscarinic acetylcholine receptors in macaque V1 are most frequently expressed by parvalbumin-immunoreactive neurons. J. Comp. Neurol. *507*, 1748–1762.

30. Disney, A.A., Aoki, C., and Hawken, M.J. (2012). Cholinergic suppression of visual responses in primate V1 is mediated by GABAergic inhibition. J. Neurophysiol. *108*, 1907–1923.

31. Carandini, M., and Heeger, D.J. (2011). Normalization as a canonical neural computation. Nat. Rev. Neurosci. *13*, 51–62.

32. Heeger, D.J. (1992). Normalization of cell responses in cat striate cortex. Vis. Neurosci. *9*, 181–197.

33. Reynolds, J.H., and Heeger, D.J. (2009). The normalization model of attention. Neuron *61*, 168–185.

34. Lee, J., and Maunsell, J.H.R. (2010). The effect of attention on neuronal responses to high and low contrast stimuli. J. Neurophysiol. *104*, 960–971.

35. Prusky, G.T., Shaw, C., and Cynader, M.S. (1987). Nicotine receptors are located on lateral geniculate nucleus terminals in cat visual cortex. Brain Res. *412*, 131–138.

36. Gil, Z., Connors, B.W., and Amitai, Y. (1997). Differential regulation of neocortical synapses by

neuromodulators and activity. Neuron *19*, 679–686.

37. Hsieh, C.Y., Cruikshank, S.J., and Metherate, R. (2000). Differential modulation of auditory thalamocortical and intracortical synaptic transmission by cholinergic agonist. Brain Res. *880*, 51–64.

38. Kruglikov, I., and Rudy, B. (2008). Perisomatic GABA release and thalamocortical integration onto neocortical excitatory cells are regulated by neuromodulators. Neuron *58*, 911–924.

39. Kimura, F., Fukuda, M., and Tsumoto, T. (1999). Acetylcholine suppresses the spread of excitation in the visual cortex revealed by optical recording: possible differential effect depending on the source of input. Eur. J. Neurosci. *11*, 3597–3609.

40. Reynolds, J.H., Pasternak, T., and Desimone, R. (2000). Attention increases sensitivity of V4 neurons. Neuron *26*, 703–714.

41. Williford, T., and Maunsell, J.H.R. (2006). Effects of spatial attention on contrast response functions in macaque area V4. J. Neurophysiol. *96*, 40–54.

42. Carandini, M., Heeger, D.J., and Movshon, J.A. (1997). Linearity and normalization in simple cells of the macaque primary visual cortex. J. Neurosci. *17*, 8621–8644.

43. De Valois, R.L., William Yund, E., and Hepler, N. (1982). The orientation and direction selectivity of cells in macaque visual cortex. Vision Res. *22*, 531–544.

44. Ringach, D.L., Shapley, R.M., and Hawken, M.J. (2002). Orientation selectivity in macaque V1: Diversity and laminar dependence. J. Neurosci. *22*, 5639–5651.

45. Disney, A.A. (2021). Neuromodulatory Control of Early Visual Processing in Macaque. Annu Rev Vis Sci *7*, 181–199.

46. Coppola, J.J., Ward, N.J., Jadi, M.P., and Disney, A.A. (2016). Modulatory compartments in cortex and local regulation of cholinergic tone. J. Physiol. Paris *110*, 3–9.

47. Ling, S., and Carrasco, M. (2006). Sustained and transient covert attention enhance the signal via different contrast response functions. Vision Res. *46*, 1210–1220.